

Quantized Pulse Propagation in Josephson Junction Arrays

Christine A. Donnelly , Justus A. Brevik , Nathan E. Flowers-Jacobs , Anna E. Fox , *Senior Member, IEEE*, Paul D. Dresselhaus , Peter F. Hopkins , *Senior Member, IEEE*, and Samuel P. Benz , *Fellow, IEEE*

Abstract—We present time-domain electrical measurements and simulations of the quantized voltage pulses that are generated from series-connected Josephson junction (JJ) arrays. The transmission delay of the JJ array can lead to a broadening of the net output pulse, depending on the direction of the output pulse propagation relative to the input bias pulse. To demonstrate this, we compare time-domain measurements of output pulses from radio-frequency Josephson arbitrary waveform synthesizer (RF-JAWS) circuits fabricated with two different output measurement configurations, so that the backward-propagating and forward-propagating pulses can be measured. Measurements were made on arrays with 1200 and 3600 JJs and show that the net backward-propagating output pulse is broadened by timing delays in the JJ array, whereas the net forward-propagating output pulse is insensitive to delay effects and can theoretically be further scaled to longer JJ array lengths without significant output pulse broadening. These measurements match well with simulations and confirm the expectation that the net output pulses arise from the time-delayed superposition of individual JJ output pulses from the series array of JJs. The measurements and analysis shown here have important implications for the realization of RF-JAWS circuits to be used as quantum-based reference sources for communications metrology.

Index Terms—Digital-analog conversion, Josephson junction (JJ) arrays, power measurement, quantization, signal synthesis, superconducting integrated circuits, superconducting devices.

I. INTRODUCTION

THE Josephson arbitrary waveform synthesizer (JAWS) is a superconducting digital-to-analog converter used to synthesize quantum-based ac voltage waveforms for metrology applications [1], [2]. The JAWS circuit contains a series array of Josephson junctions (JJs) that produces a quantized output pulse in response to each programmed input drive pulse. The net quantized output pulse from the array of JJs is a superposition of the individual pulses from each JJ in the array.

Manuscript received April 21, 2019; revised June 15, 2019; accepted June 17, 2019. Date of publication July 23, 2019; date of current version September 10, 2019. The work of C. Donnelly is supported by NIST Graduate Student Measurement Science and Engineering fellowship. This article was recommended by Associate Editor Igor V. Vernik. (*Corresponding author: Christine Donnelly.*)

C. A. Donnelly is with the National Institute of Standards and Technology, Boulder, CO 80305 USA, and also with Stanford University, Department of Electrical Engineering, Stanford, CA 94305 USA (e-mail: cdonnelly0626@gmail.com).

J. A. Brevik, N. E. Flowers-Jacobs, A. E. Fox, P. D. Dresselhaus, P. F. Hopkins, and S. P. Benz are with the National Institute of Standards and Technology, Boulder, CO 80305 USA.

Color versions of one or more of the figures in this article are available online at <http://ieeexplore.ieee.org>.

Digital Object Identifier 10.1109/TASC.2019.2929481

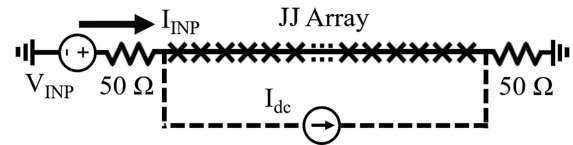


Fig. 1. Schematic of a series-connected JJ array for a JAWS system. In addition to the JJ array, the JAWS system includes an external input current pulse drive I_{INP} that is generated by a voltage source V_{INP} in series with a 50Ω resistor, as well as a dc bias current I_{dc} . The array is terminated in a 50Ω resistor. The output voltage port, which can be added in a number of different ways (see Fig. 4 for examples), is not included in this schematic.

The JAWS system has already been used to synthesize quantum-accurate audio-frequency voltage waveforms for a variety of applications, including measurement of harmonic distortion, spurious-free dynamic range, and noise in commercial electronics [3], [4]; calibration of commercial voltage sources [5]; and thermal voltage converters [6]; and harmonic phase analysis for distorted waveforms [7].

Efforts are currently ongoing at NIST to develop a radio-frequency JAWS (RF-JAWS) system for synthesis of waveforms at gigahertz frequencies to be used as a reference standard [8], [9]. Such a system would supplement existing metrology tools [10], [11] and would serve as the first quantum-based waveform source for communications-frequency waveform calibrations. However, as JAWS circuits are developed and optimized for synthesis of higher output frequencies, a number of new design issues have arisen that have the potential to compromise output waveform accuracy [9], [12]. This article focuses on the particular issue of the broadening of the net output voltage pulse due to transmission delays in series-connected JJ arrays. A schematic of a simple series-connected JJ array for a JAWS circuit is shown in Fig. 1. Delays result both from the propagation of the input bias pulse I_{INP} through the array, which causes individual JJs to create output voltage pulses at different times, and also from the propagation of the individual JJ pulses to the output port. If these array transmission delays cause the individual JJ pulses to arrive at the JAWS output port at different times, then the net output voltage pulse will be broader than that of an individual JJ output pulse.

The array transmission delay increases as the number of series-connected JJs and the corresponding array length increases, reaching a value of approximately 100 ps for a typical array of length 13 mm (~ 6000 JJs). Unlike at audio frequencies, this delay at gigahertz frequencies is not negligible relative to

the waveform period, and will be a significant source of error if the net array output pulse is broadened by the full array transmission delay period. This source of error will become particularly important as RF-JAWS circuits are scaled to longer array lengths in order to increase the number of JJs and achieve higher output waveform power [9].

The measurements and analysis in this article are intended to 1) measure time-domain output pulse broadening caused by transmission delays in JJ arrays, and 2) identify a circuit design that maintains a phase-aligned superposition of individual output pulses free of pulse broadening, regardless of array length. Previous measurements of single flux quantum (SFQ) output pulses from individual JJs in Josephson transmission lines have been reported using either electronic measurements or optoelectronic techniques [13]–[15]. This article reports the first electrical measurements of output superposition pulses from a series-connected array of thousands of JJs driven by a room-temperature pulse bias current source.

This article is organized as follows. In Section II, a brief overview is provided of JAWS operational principles and of new RF-JAWS circuit design challenges that motivated the experimental investigations described in this article. In Section III, the dynamics of quantized pulse propagation in an RF-JAWS circuit is described for the case of a single JJ. In Section IV, a mathematical description is provided for the details of quantized pulse propagation and superposition in arrays of JJs. Next, in Section V, two different RF-JAWS circuit designs are presented that differ by the location of the output port and allow the pulse propagation asymmetry of the JJ arrays to be measured. Experimental methods for measuring time-resolved output pulses are described in Section VI, while results are shown in Section VII and are compared to circuit simulations. Finally, discussion of the experimental results is given in Section VIII and Section IX concludes this article.

II. RF-JAWS OPERATIONAL PRINCIPLES AND DESIGN CHALLENGES

The standard RF-JAWS circuit design, shown in Fig. 1, includes an array of JJs that responds to an external pulsed current drive signal (I_{INP}) by producing output voltage pulses with quantized time-integrated area. The system is operating correctly when the JJs are “quantum-locked” to the drive and an integer number n of quantized output pulses are synthesized in response to each input drive pulse over a range of input drive pulse parameters and values of dc current (I_{dc}) supplied to the JJ array [9], [16], [17]. The time-integrated voltage area of each quantized output pulse is equal to $\int p(t)dt = nN_{JJ}\Phi_0$, where $p(t)$ is the voltage generated across each JJ, N_{JJ} is the number of JJs in the array, and $\Phi_0 \equiv h/2e$ is the magnetic flux quantum. For the purpose of quantized waveform synthesis, the JAWS system is typically operated within the $n = 1$ “quantum-locked range” (QLR). For the experiments described in this article, the QLR is typically measured as a function of I_{dc} while all other input parameters are held fixed.

Full waveforms are synthesized from the RF-JAWS circuits by encoding the target waveforms with a single-bit digital delta-sigma encoding, and triggering a quantized output pulse from the JJ array at each clock cycle in which “1” is present in the digital encoding. Mathematically, the output waveform from a JAWS circuit is a convolution of the quantized-area output pulse shape with the full digital code. In the frequency domain, this means that the output waveform frequency content is scaled by the Fourier transform of the array output pulses [9], [12].

In the JAWS circuits designed at NIST, the JJs are connected in series along the center conductor of a horizontal coplanar waveguide (CPW) with characteristic impedance Z_0 . The JJs are fabricated in vertical stacks of three JJs per stack, where the spacing between stacks along the CPW center conductor is approximately $6.5 \mu\text{m}$ for the standard JAWS circuit design. The drive pulses are applied to the input end of the JJ array from a room-temperature voltage source with output impedance of 50Ω . For audio-frequency JAWS circuit designs, the CPW characteristic impedance is tapered along the array length to compensate for microwave attenuation caused by shunt resistance of JJs in the array, and the array is terminated in a resistor approximately matched to the final tapered value of Z_0 [18]. In contrast, for RF-JAWS circuits the value of $Z_0 = 50 \Omega$ is kept constant along the array length and the array is terminated, either on-chip or off-chip, by a matched 50Ω resistance (as shown in Fig. 1).

In circuits designed for audio-frequency JAWS measurements, the voltage pulse $p(t)$ synthesized across the JJ array is measured by placing inductively filtered voltage taps directly across the array and measuring the low-frequency components of $p(t)$ across the high-impedance load of an external digitizer. However, two potential concerns with this measurement approach have been identified when designing JAWS systems to synthesize radio-frequency output waveforms. The first concern is that the high-impedance measurement configuration contains a mismatch between the output 50Ω cabling and the high-impedance measurement load, resulting in standing waves on the output cabling that become a significant source of error as frequency increases. This concern has been extensively discussed in the context of low-frequency $< 1 \text{ MHz}$ JAWS measurements [19]–[25]. To avoid a mismatch, the synthesized voltage can instead be measured across a 50Ω resistor at either the input or termination end of the array, as will be discussed throughout this article. The second concern is that the time-of-flight of synthesized pulses traveling along the JJ array itself is nonnegligible relative to the output waveform period for synthesis of radio-frequency waveforms.

III. QUANTIZED PULSE PROPAGATION FROM A SINGLE JJ

Both of the RF-JAWS design concerns introduced above require a detailed analysis of the dynamics governing quantized pulse propagation from the location of pulse synthesis in the distributed JAWS circuits to the load of a device under test (DUT). This section will consider propagation of pulses generated from a single JJ within a CPW, while Section IV will extend this

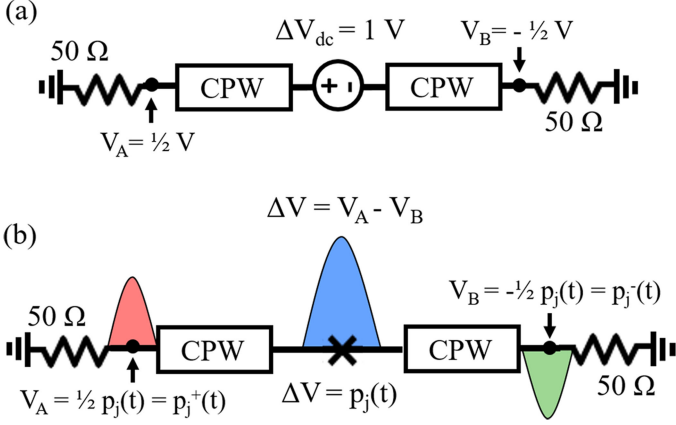


Fig. 2. (a) Splitting of the dc voltage generated across an ideal voltage source that had both positive and negative nodes connected to ground via CPW and resistors of equal impedance. (b) Splitting of the synthesized pulse voltage generated across a single JJ that is similarly connected to ground via paths of equal impedance at both the positive and negative terminals.

analysis to a full description of pulses generated from arrays containing multiple JJs.

Consider first the case of a low-frequency or dc voltage source with both its positive and negative nodes connected to ground via $50\ \Omega$ transmission line segments in series with matched $50\ \Omega$ termination resistors, as shown in Fig. 2(a). By symmetry, a dc voltage of 1 V generated across such a voltage source would “split” across the nodes V_A and V_B of the positive and negative node termination resistors, respectively, such that $V_A = 1/2\ \text{V}$, $V_B = -1/2\ \text{V}$, and $V_A - V_B = 1\ \text{V}$.

Next, consider the case in which the ideal voltage source is replaced by a single JJ. When the JJ is excited by input drive pulses, it essentially acts as a quantized-area pulse voltage source with $\Delta V = p_j(t)$, as shown in the cartoon of the quantized voltage pulse in Fig. 2(b). Here, the subscript j denotes the response of a single JJ. As was the case for the dc voltage source described above, $p_j(t)$ splits into $p_j^+(t) = p_j(t)/2$ at node V_A measured across the positive-terminal output resistor, and $p_j^-(t) = -p_j(t)/2$ at node V_B across the negative-terminal output resistor. The pulse area of Φ_0 splits in a ratio of 50% between output resistors if both the positive and negative nodes of the JJ are connected to ground via paths with equal impedances. More generally, the pulse area splits according to the impedance ratio between the two paths to ground, which determines a voltage division ratio for JJ pulses across the two termination resistors. Regardless of exact splitting ratios, it remains true that within the $n = 1$ QLR, $\int [p_j^+(t) - p_j^-(t)] dt = \int p_j(t) dt = \Phi_0$ per JJ.

IV. QUANTIZED PULSE PROPAGATION FROM MULTIPLE-JJ ARRAYS

JAWS circuit designs contain hundreds or thousands of JJs connected in series along the JJ array, such that the total propagation delay between JJs from start to end of the array can grow to 100 ps or greater. The quantized output voltage pulses from each individual JJ add in superposition, and the shape of this net pulse measured at output nodes V_A and V_B is affected by

the transmission delay of the array. Actual JJ arrays fabricated at NIST use vertical stacks of three JJs per stack rather than single JJs [26], and for the purposes of this article, we assume that each JJ in a stack pulses simultaneously. The JJ array CPW has a propagation velocity of approximately $v_p \approx 0.43c$, where c is the speed of light in vacuum and v_p is determined from simulations of the CPW inductance and capacitance per unit length of $0.4\ \mu\text{H}/\text{m}$ and $150\ \text{pF}/\text{m}$, respectively.

The input pulse to the JJ array has a definite direction of travel from the start of the array to the termination resistor, and it is subject to the same propagation delay t_d as it travels to each sequential JJ and triggers an output pulse $p_j(t)$. As a result, an asymmetry is produced in the net quantized pulse shape measured across node V_A versus V_B . The propagation direction of the input drive pulses I_{INP} and quantized half-pulses $p_j^-(t)$ will be referred to as the “forward-propagating” direction throughout this article, while the direction of the quantized half-pulses $p_j^+(t)$ is the “backward-propagating” direction. For simplicity, we assume for this analysis that each JJ has an identical response function $p_j(t)$.

The forward-propagating pulses $p_j^-(t)$ travel at the same speed and in the same direction as the input drive pulses. A pulse synthesized from the first JJ in the array at time $t = 0$ centered at position $x = 0$ will travel along the array’s x -axis as time evolves, according to $p_j^-(x, t) = p_j^-(x - v_p t)$. As the input drive pulse continues to travel along the array, the pulses synthesized from downstream JJs have both an initial time offset and position offset from the first output pulse. When the input drive pulse has reached the m th JJ in the array at time $t = m t_d$, the accumulated forward-propagating JJ-synthesized pulse $p(x, t)$ is expressed mathematically as

$$\begin{aligned} p(x, t)|_{t=mt_d} &= \sum_{k=1}^m p_j^-((x - k v_p t_d) - v_p (t - k t_d))|_{t=mt_d} \\ &= m p_j^-(x - v_p t)|_{t=mt_d} \\ &= m p_j^-(x - m v_p t_d). \end{aligned} \quad (1)$$

Equation (1) shows that because the “upstream” synthesized quantized pulses propagate synchronously with the input drive pulse, the pulses add coherently and are simply shifted along the x -axis with growing net amplitude as time progresses. The time evolution of this forward-propagating negative half-pulse waveform is shown in Fig. 3 at four timesteps of pulse generation along a series array of 3600 JJs, arranged in 1200 stacks of three JJs per stack. The figure was generated assuming a delay between JJ stacks of 200 fs to match experimental circuit designs that will be described in Section V. For the illustrative purposes of this figure, a simple Gaussian pulse shape with pulsewidth of 50 ps was assumed. The negative-polarity forward-propagating pulse waveform (green in Fig. 3) retains the same pulsewidth but grows in amplitude as time progresses.

In contrast, the backward-propagating pulses (red in Fig. 3) travel along the x -axis according to $p_j^+(x, t) = p_j^+(x + v_p t)$. The initial time and position offset of the backward-propagating pulse generated from the k th JJ relative to the first JJ is the

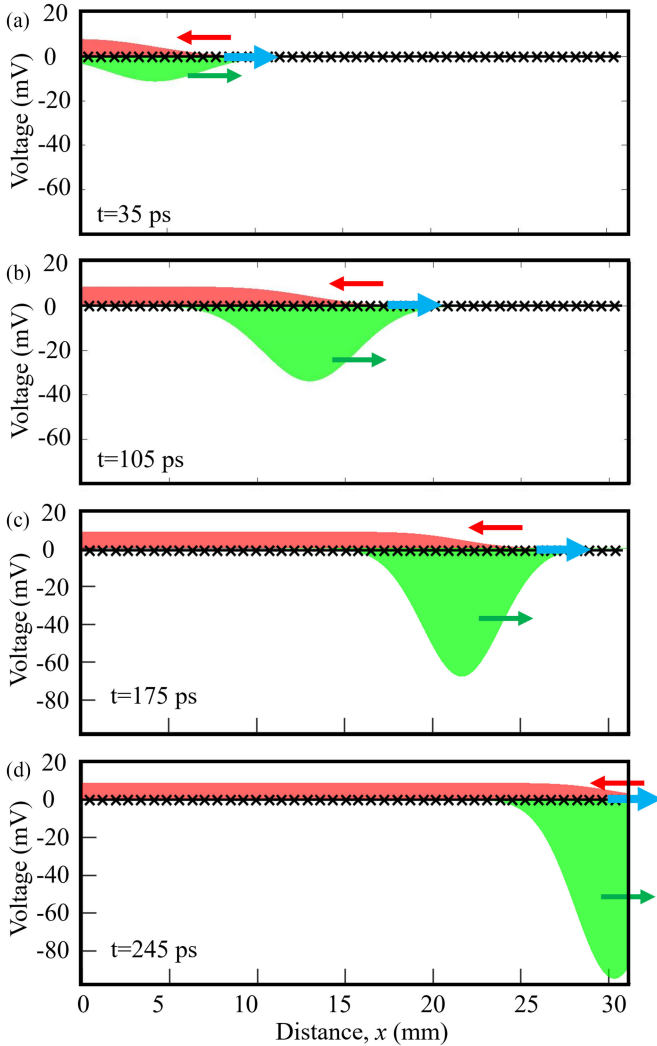


Fig. 3. Cartoon of a 3600 JJ array at four timesteps showing the negative amplitude forward-propagating and positive amplitude backward-propagating pulse waveforms generated by the JJs in response to a single input drive pulse. The thicker arrow indicates the direction and progression of the input drive pulse (not shown). As time progresses, the forward-propagating pulse traveling to the right retains the same pulsewidth but grows in amplitude while the backward-propagating pulse traveling to the left retains a steady-state amplitude but grows in width. The JJ array schematic shown in the figure is not to scale.

same as for the forward-propagating case. Overall, the accumulated backward-propagating pulse waveform at time $t = mt_d$ is described by

$$\begin{aligned}
 p(x, t)|_{t=mt_d} &= \sum_{k=1}^m p_j^+((x - kv_p t_d) + v_p(t - kt_d))|_{t=mt_d} \\
 &= \sum_{k=1}^m p_j^+(x + v_p t - 2kv_p t_d)|_{t=mt_d} \\
 &= \sum_{k=1}^m p_j^+(x + v_p t_d(m - 2k)). \quad (2)
 \end{aligned}$$

Equation (2) shows that the backward-propagating synthesized pulses from individual JJs do *not* add coherently but are all shifted along the array x -axis by $2v_p t_d$ relative to one another (where $v_p t_d$ is, by definition, equal to the spacing between JJs).

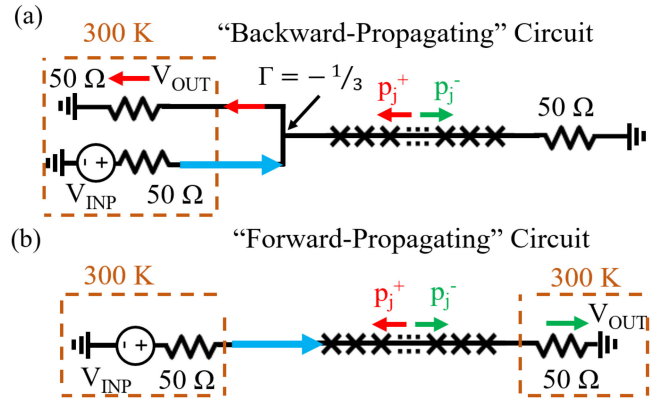


Fig. 4. Schematics of test circuits designed for the purpose of measuring broadband output pulse waveforms. The circuits had either 400 stacks or 1200 stacks of three JJs spaced apart by $26 \mu\text{m}$. The room-temperature components are indicated in dashed boxes. The blue arrows indicate the direction of travel of the input drive pulse.

Because the output pulsewidth is on the order of 50 ps for JJs with $I_C R_N = 40 \mu\text{V}$ and the delay between JJs is approximately 200 fs for the circuits measured in this article, the pulses from individual JJs blend together and form a steady-state backward-propagating waveform along the array, as shown in Fig. 3. The backward-propagating pulse waveform grows in width along the JJ array as the drive pulse propagates to the termination, but remains at the same steady-state amplitude. The rising edge of this waveform begins as soon as the first JJ in the array produces an SFQ pulse and the falling edge does not occur until almost twice the total array propagation delay; the drive pulse must first reach the final JJ and then the pulse generated by this JJ has to travel backward to the beginning of the array.

V. CIRCUIT DESIGNS FOR PULSE PROPAGATION COMPARISON MEASUREMENTS

In order to verify the analytical description of pulse propagation described above, a set of forward-propagating and backward-propagating pulse circuits were fabricated for experimental measurements. The goal of the experiments was to measure single output pulse waveforms and observe the differences in $p(t)$ with the two different measurement configurations. For the purpose of these measurements, the spacing between JJ stacks was increased to $26 \mu\text{m}$ (corresponding to a delay between stacks of $t_d \approx 200$ fs) so that differences in forward-propagating and backward-propagating output pulsewidths could be more easily measured. Two different array lengths were also measured to confirm the linear dependence of the pulse broadening on array length. One pair of circuits used 400 stacks of three JJs, for a total count of $N_{\text{JJ}} = 1200$ and a one-way array propagation delay, including routing bends, of approximately 83 ps. The second pair of circuits used 1200 stacks of three JJs, for a total count of $N_{\text{JJ}} = 3600$ and a total one-way propagation delay of approximately 250 ps.

The schematics for the pair of test circuits are shown in Fig. 4. As shown in this figure, the backward-propagating circuit layout included an on-chip 50Ω array termination resistor, while all 50Ω resistors were located off-chip for the forward-propagating

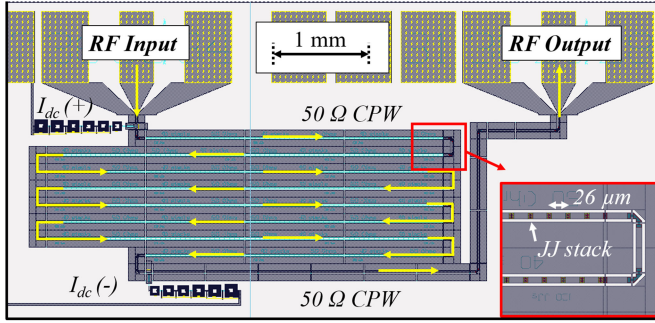


Fig. 5. Layout of forward-propagating waveform measurement circuit with an array of 3600 JJs grouped into vertical stacks of 3 JJs per stack spaced apart by $26 \mu\text{m}$. The RF input and output lines and dc bias lines are also indicated.

circuit design. The physical layout for the forward-propagating measurement circuit with 3600 JJs (1200 JJ stacks) is shown in Fig. 5. All of the arrays also included inductively-filtered bias taps such that dc bias currents could be applied across the array. Typically, RF-JAWS circuits also include frequency-selective filters arranged in a reflectionless filter configuration [8], [9] to separate the input drive frequency content from the synthesized signal frequency content while maintaining 50Ω impedance matching. However, all filters were removed for the circuit designs used in this article to allow the broadband output pulse waveforms to be measured. The removal of the reflectionless filter configuration required that a three-way unfiltered microwave tee be included in the backward-propagating pulse circuit design, as shown in Fig. 4. The microwave tee presents an effective 25Ω impedance to signals arriving from any of its three 50Ω ports and, therefore, has a nonzero reflection coefficient and a nonunity transmission coefficient. It was thus expected that only $2/3$ of the backward-propagating JJ-synthesized waveform amplitude would be measured across the load of the DUT for this circuit, while the remaining third would be reflected back to the JJ array and terminated by the on-chip 50Ω array termination resistor.

VI. EXPERIMENTAL METHODS

The output pulse waveforms were measured with a 50 GHz bandwidth sampling oscilloscope. A zero-compensation [27] input pulse shape with center lobe pulsewidth of approximately 50 ps was used to drive the output pulses from the JJs. The broadband input drive pulse also reaches the oscilloscope, and this “feedthrough” signal from the input pulses is much larger than the JJ-synthesized output pulse signal. In order to subtract the input drive pulse feedthrough, the bias current I_{dc} was set to a value such that the combination of input drive pulse and input dc current would not drive any quantized pulses from the JJs in the array ($n = 0$ output state). Under these bias conditions, a baseline measurement was taken of the circuit output in the presence of the full input drive signal. Next, the input drive was not changed but I_{dc} was set to an operational value within the range for generating single quantized pulses ($n = 1$ output state) and the circuit output was again measured. The generated quantized pulse signal was recovered by subtracting the initial

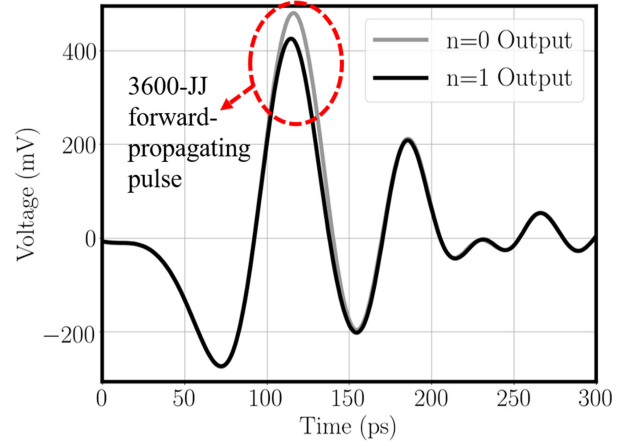


Fig. 6. Measured waveforms from the $n = 0$ and $n = 1$ output states with the 3600-JJ forward-propagating broadband measurement circuit. The majority of the signal is input drive feedthrough, and the difference between the traces is due to the net quantized output pulse from the JJs.

$n = 0$ measurement result from the second $n = 1$ measurement result. This measurement and subtraction sequence was repeated 400 times and was averaged to reduce measurement noise. The relative magnitude of the difference signal compared to the total output signal is shown in Fig. 6 for the 3600-JJ forward-propagating circuit. As shown in the figure, the peak magnitude of the difference signal is less than 15% of the peak input pulse feedthrough signal magnitude for this circuit.

VII. EXPERIMENTAL RESULTS

The measured quantized pulse traces from the two circuit configurations with 1200 JJs are shown in Fig. 7(a) and (b). The forward-propagating pulse waveform had a peak measured amplitude of approximately 28 mV and a pulsewidth of approximately 40 ps, while the backward-propagating pulse waveform was extended to a pulsewidth of approximately 180 ps with a reduced amplitude of 6 mV. Next, the measured pulse traces from the two circuit configurations with 3600 JJs are shown in Fig. 7(c) and (d). In this case, with the number of JJs and corresponding array length increased by a factor of three, the forward-propagating waveform retained nearly the same pulsewidth of 40 ps as the 1200-JJ circuit output pulses but grew in amplitude by a factor of approximately three to a peak amplitude of 85 mV. In contrast, the backward-propagating waveform retained nearly the same peak amplitude as the 1200-JJ circuit but instead grew in pulsewidth by a factor of approximately 3–520 ps.

WRspice¹ [28] simulations of the two circuit configurations are also shown in Fig. 7; a reasonable match was observed between simulations and experimental data. The JJ output pulses were simulated in WRspice using a resistively and capacitively shunted JJ model and did not assume the simple Gaussian pulse shape shown in Fig. 3. The WRspice simulations used the measured oscilloscope traces of the input pulses to drive, in

¹Specific software products are identified in order to adequately specify the simulation procedure. Such identification does not imply recommendation or endorsement by NIST, nor does it imply that the software identified is necessarily the best available for the purpose.

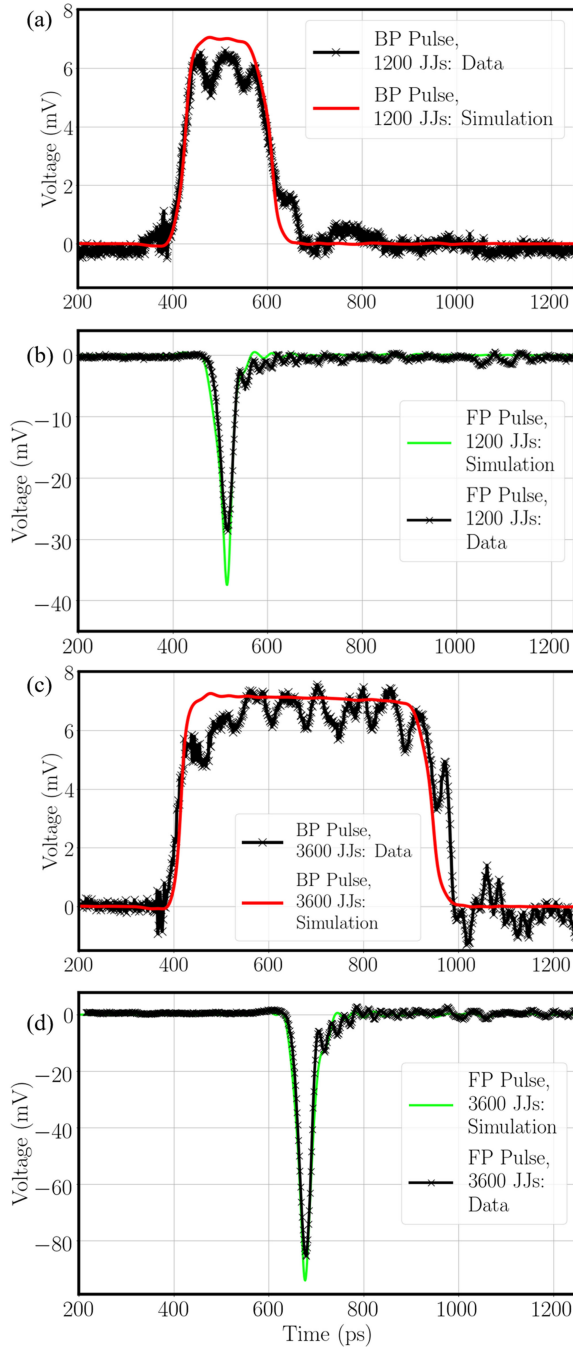


Fig. 7. (a) Measured and simulated backward-propagating pulse waveforms from the 1200-JJ RF-JAWS circuits. (b) Measured and simulated forward-propagating pulse output waveforms from the 1200-JJ RF-JAWS circuits. (c) Measured and simulated backward-propagating pulse waveforms in the 3600-JJ RF-JAWS circuits. The measured pulsewidth increased from approximately 180 ps to approximately 520 ps when the array length was increased by a factor of three. (d) Measured and simulated forward-propagating pulse waveforms from the 3600-JJ RF-JAWS circuits. The measured peak pulse waveform amplitude increased from 28 to 85 mV when the JJ array length was increased.

simulation, series-connected arrays of JJs in both the forward-propagating and backward-propagating circuit configurations. In the simulations, each stack of JJs was separated from adjacent stacks by a short transmission line segment with $Z_0 = 50 \Omega$ and $t_d = 200$ fs. The JJs were simulated using $I_C = 8$ mA

and $I_C R_N = 40 \mu\text{V}$, which were close to the measured values for the JJs used in experiments. The overall amplitude of the input drive pulses was left as a free simulation parameter; this parameter affects both the peak amplitude of the simulated pulses and the nature of the overshoot at the end of the pulse, and a balance between these two factors was used to best match the simulations to the experimental measurements. Finally, just as in the measurements, the simulations subtracted an output waveform at the $n = 0$ output state from the $n = 1$ output state in order to recover the simulated quantized pulses and remove feedthrough of the input drive pulse. For the purpose of all figures, both the measured and simulated backward-propagating pulse waveforms were multiplied by an overall scale factor of $3/2$ to account for the expected $2/3$ transmission factor inherent in the circuit design and allow a more relevant comparison with the forward-propagating data and simulations.

The reason for the ringing in the experimental data relative to the simulation data is most likely due to both 1) reflections at circuit structures such as bends, taps, and launches in the array and connectors, including the microwave input and output ports labeled “RF input” and “RF output” in Fig. 5, and 2) multiple reflections and standing waves on the off-chip output cabling caused by any impedance mismatches between the output cabling and the measurement load. The effects of these on-chip and off-chip reflections were not modeled in the simulations. The slight downward slope in the simulated backward-propagating pulse amplitudes is attributed to microwave attenuation caused by the R_N of the JJs along the length of the array, which causes a reduced peak amplitude in the JJ pulses generated later in time via two physical mechanisms. First, as was briefly mentioned in Section II, the input drive pulses experience dissipation from the finite shunt resistance R_N of JJs along the array and, therefore, have higher peak current at the beginning of the array compared to the peak current at the end of the array. Input pulses with higher peak current drive lead to output JJ pulses with slightly narrower pulsewidth and higher peak voltage, and these sharper output pulses reach the load of the DUT earlier in time with the backward-propagating circuit configuration. As time progresses, the output JJ pulses that reach the load of the DUT have slightly wider pulsewidth and lower peak voltage. Second, the quantized output pulses at the end of the array experience peak voltage attenuation, that is, low pass filtering, while traveling backwards through other JJs to the load of the backward-propagating circuit DUT, which exacerbates the asymmetry in simulated voltage amplitude from start to end of the backward-propagating pulse.

Similar effects explain why the simulated pulse amplitude for the forward-propagating circuit does not increase by a full factor of three when the number of JJ changes from 1200 to 3600. According to simulation, there is also peak attenuation of the forward-propagating pulses as they travel down longer arrays due to R_N of the JJs in the array. The ratio of the peak amplitudes in the simulations is not reproduced in the measurement because the peak attenuation is dominated by the output cabling and SMA connectors and is similar for both array lengths.

It should be noted that, although the theoretical integrated area of the pulses produced by the JJ array is equal to $N_{JJ} \Phi_0$, the measured pulse areas reported in this article are not expected to

be exactly $N_{JJ}\Phi_0/2$ because the pulse splitting in the array, as well as the external transfer function to the output measurement system, are not fully calibrated. The measured pulse areas are also sensitive to any small dc offset in the oscilloscope measurements. Regardless, after accounting for the $2/3$ transmission factor of the backward-propagating circuit configuration and subtracting the approximate oscilloscope offset determined from the initial quiescent portions of the measured pulse waveforms, the pulse areas are found to match the expected quantized values to within $\pm 10\%$. It is also worth emphasizing that although the output transfer function and resulting measured pulse areas were not fully calibrated, we nonetheless verified a stable operating range over which the measured pulse areas were invariant with respect to changes in input bias parameters. Within this range, the JJ array was producing a constant number $n = 1$ of output pulses per JJ per input bias pulse and was, therefore, considered to be quantum-locked to the input pulse drive [9], [16], [17]. In the future, performing quantum-based measurements using RF-JAWS systems will require both a quantum-locked system and a fully calibrated transfer function between the JJ arrays and the DUTs.

VIII. DISCUSSION

The shape of the output pulses in the RF-JAWS circuits directly affects the error in the fundamental tone power of the output waveforms [9], [12]. As discussed in Section II, the RF-JAWS output waveforms are a time-domain convolution of a digital waveform encoding with the single-pulse array output waveform. Using the mapping from time-domain convolution to frequency-domain multiplication, the spectrum of the RF-JAWS synthesized output waveforms is therefore given by

$$V_{JJ}(f) = P(f)W(f) \quad (3)$$

where $V_{JJ}(f)$ is the Fourier transform of the full output waveform, $P(f)$ is the Fourier transform of each array output pulse, and $W(f)$ is the calculable Fourier transform of the digital encoding. The quantized area of each output pulse ensures that the dc component $P(0)$ is quantized

$$P(0) = \Phi_0 N_{JJ} / (2T) \quad (4)$$

where N_{JJ} was previously defined as the number of JJs in the array, T is the clock period used for driving the RF-JAWS system with the input code, and the factor of two is based on the assumption that the quantized pulses from individual JJ stacks split as described above and are measured either in the forward-propagating or backward-propagating mode. While (4) always provides a calculable definition of $P(0)$ regardless of pulse shape, the value of $P(f)$ at any nonzero frequency deviates from the quantized dc value, and the nature of this deviation depends on the pulse shape. The error in output power due to a particular pulse Fourier transform $P(f)$ is calculated as $[P(f)^2 - P(0)^2]/P(0)^2$. We also note that the phase of $P(f)$ varies with frequency and this dependence could become a source of error for wideband RF-JAWS applications, where the relative phase between synthesized tones is important. The measured frequency-dependent phase of $P(f)$

is directly affected by dispersion in the JJ array and output transmission lines. Furthermore, both the magnitude and phase of $P(f)$ are indirectly affected by dispersion in the input drive transmission path, altering the shape of the input drive pulses and, therefore, the output response pulses of the JJs.

In the case of the forward-propagating RF-JAWS circuit, it has been shown that the measured pulse shape remains narrow in time regardless of array length and is limited by the characteristic frequency of JJs in the RF-JAWS circuits. The JJs used in these experiments with $I_C R_N = 40 \mu\text{V}$ have characteristic frequency of approximately 20 GHz, and the deviation between $P(f)$ and $P(0)$ is small until f approaches this characteristic frequency [9], [12]. To further reduce the error between $P(f)$ and $P(0)$ at a given frequency, the characteristic frequency of the JJs could be increased.

In contrast, in the case of the backward-propagating RF-JAWS measurement configuration, the pulse shape continues to widen as array length increases. The output pulses from the backward-propagating RF-JAWS circuits are well-approximated by rectangular pulse functions with pulsewidth of $2T_d$, where T_d is the full array transmission delay, such that the magnitude of $P(f)$ is scaled by $|\text{sinc}(2\pi f T_d)|$ relative to $P(0)$, where $\text{sinc}(x)$ is defined as $\sin(x)/x$. For a standard RF-JAWS circuit layout, defined as $6.5 \mu\text{m}$ spacing between stacks of three JJs, with 1002 JJs and $2T_d = 33$ ps, the fractional error in output power of the backward-propagating waveform due to pulsewidth broadening would therefore be equal to -0.4% at 1 GHz. For a layout with 6000 JJs and $2T_d = 200$ ps, the error would increase to -13% .

At sufficiently low frequencies such that $f \ll (2\pi T_d)^{-1}$, the relationship $|P(f)|^2 \approx |\text{sinc}(2\pi f T_d)|^2$ can be further approximated by the power series expansion for $|\text{sinc}(x)|^2$ about $x = 0$ to obtain the relationship $|P(f)|^2 \approx 1 - (2\pi f T_d)^2/3$. The fractional error ϵ in JAWS backward-propagating waveform output power at low synthesis frequencies, with corresponding waveform period much larger than the array transmission delay time, is therefore given by

$$\epsilon \approx \frac{(2\pi f T_d)^2}{3}. \quad (5)$$

For a standard array with 12 000 JJs and $2T_d = 400$ ps, the equivalent fractional voltage error $\epsilon/2 \lesssim 1$ part in 10^6 (1 part per million) for synthesis frequencies $f \lesssim 2$ MHz.

Therefore, only low-frequency waveforms or waveforms generated by short JJ arrays with lower transmission delay can be measured in a backward-propagating configuration without incurring a significant error penalty.

IX. CONCLUSION

In this article, we have shown that the output quantized-area pulses from series-connected arrays containing N_{JJ} JJs only add coherently in the forward propagation direction when the arrays are driven by an external current pulse. In particular, for the circuits presented here the forward-propagating pulse waveforms add synchronously such that the net output forward-propagating waveform has a pulsewidth similar to a

single-JJ SFQ pulse but with amplitude multiplied by $N_{JJ}/2$, while the backward-propagating pulse waveforms are affected by the array transmission delay and do not add synchronously. This asymmetry between output waveforms was first postulated based on simulation analysis and was next verified in experimental measurements of output pulses from arrays of 1200 JJs and 3600 JJs, arranged in both the forward-propagating and backward-propagating measurement configurations. While the forward-propagating output pulses retained the same pulsewidth but grew in amplitude proportional to the number of JJs in the array, the backward-propagating output pulses grew in *pulsewidth* proportional to the physical length of the JJ array, but retained approximately the same amplitude. These results indicate that the forward-propagating pulse measurement configuration discussed in this article will be the preferable circuit design to minimize error due to pulse shape broadening in future RF-JAWS circuits.

ACKNOWLEDGMENT

The authors would like to thank the NIST Boulder Microfabrication Facility and the NIST staff who support it for fabrication of the superconducting JAWS chip described in this paper. This work is a contribution of the U.S. government and is not subject to U.S. copyright.

REFERENCES

- [1] S. P. Benz and C. A. Hamilton, "A pulse-driven programmable Josephson voltage standard," *Appl. Phys. Lett.*, vol. 68, pp. 3171–3173, Mar. 1996.
- [2] R. Behr, O. Kieler, J. Kohlmann, F. Muller, and L. Palafox, "Development and metrological applications of Josephson arrays at PTB," *Meas. Sci. Technol.*, vol. 23, Dec. 2012, Art. no. 124002.
- [3] R. Toonen and S. Benz, "Nonlinear behavior of electronic components characterized with precision multitones from a Josephson arbitrary waveform synthesizer," *IEEE Trans. Appl. Supercond.*, vol. 19, no. 3, pp. 715–718, Jun. 2009.
- [4] R. Lapuh, B. Voljč, M. Lindič, and O. Kieler, "Keysight 3458A noise performance in DCV sampling mode," *IEEE Trans. Instrum. Meas.*, vol. 66, no. 6, pp. 1089–1094, Jun. 2017.
- [5] B. Jeanneret and S. Benz, "Application of the Josephson effect in electrical metrology," *Eur. Phys. J. Special Topics*, vol. 172, pp. 181–206, Jun. 2009.
- [6] T. E. Lipe, J. R. Kinard, Y.-H. Tang, S. P. Benz, C. J. Burroughs, and P. D. Dresselhaus, "Thermal voltage converter calibrations using a quantum ac standard," *Metrologia*, vol. 45, pp. 275–280, Jun. 2008.
- [7] D. Georgakopoulos, I. Budovsky, S. P. Benz, and G. Gubler, "Josephson arbitrary waveform synthesizer as a reference standard for the measurement of the phase of harmonics in distorted waveforms," *IEEE Trans. Instrum. Meas.*, vol. 68, no. 6, pp. 1927–1934, Jun. 2019.
- [8] P. F. Hopkins *et al.*, "RF waveform synthesizers with quantum-based voltage accuracy for communications metrology," *IEEE Trans. Appl. Supercond.*, vol. 29, no. 5, Aug. 2019, Art. no. 1301105.
- [9] C. A. Donnelly *et al.*, "1 GHz waveform synthesis with Josephson junction arrays," *IEEE Trans. Appl. Supercond.*, to be published, doi: [10.1109/TASC.2019.2932342](https://doi.org/10.1109/TASC.2019.2932342).
- [10] D. Williams *et al.*, "Covariance-based uncertainty analysis of the NIST electrooptic sampling system," *IEEE Trans. Microw. Theory Techn.*, vol. 54, no. 1, pp. 481–491, Jan. 2006.
- [11] K. A. Remley, D. F. Williams, P. D. Hale, C. Wang, J. Jargon, and Y. Park, "Millimeter-wave modulated-signal and error-vector-magnitude measurement with uncertainty," *IEEE Trans. Microw. Theory Techn.*, vol. 63, no. 5, pp. 1710–1720, May 2015.
- [12] C. A. Donnelly, J. A. Brevik, P. D. Dresselhaus, P. F. Hopkins, and S. P. Benz, "Jitter sensitivity analysis of the superconducting Josephson arbitrary waveform synthesizer," *IEEE Trans. Microw. Theory Techn.*, vol. 66, no. 11, pp. 4898–4909, Nov. 2018.
- [13] A. Matsuda and T. Kawakami, "Fluxon propagation on a Josephson transmission line," *Phys. Rev. Lett.*, vol. 51, pp. 694–697, Aug. 1983.
- [14] C. Wang, M. Currie, D. Jacobs-Perkins, M. J. Feldman, R. Sobolewski, and T. Y. Hsiang, "Optoelectronic generation and detection of single-flux-quantum pulses," *Appl. Phys. Lett.*, vol. 66, no. 24, pp. 3325–3327, 1995.
- [15] M. Maruyama *et al.*, "Observation of SFQ pulse using HTS sampler," *Phys. C: Supercond. Appl.*, vol. 463, pp. 1101–1105, 2007.
- [16] N. E. Flowers-Jacobs, A. E. Fox, P. D. Dresselhaus, R. E. Schwall, and S. P. Benz, "Two-volt Josephson arbitrary waveform synthesizer using wilkinson dividers," *IEEE Trans. Appl. Supercond.*, vol. 26, no. 6, Sep. 2016, Art. no. 1400207.
- [17] C. A. Donnelly, *Development of a Quantum-Based Superconducting Radio-Frequency Voltage Standard*. Ph.D. dissertation, Stanford, CA, USA: Stanford Univ. Press, 2019.
- [18] P. D. Dresselhaus, M. M. Elsbury, D. Olaya, C. J. Burroughs, and S. P. Benz, "10 volt programmable Josephson voltage standard circuits using NbSi-barrier junctions," *IEEE Trans. Appl. Supercond.*, vol. 21, no. 3, pp. 693–696, Jun. 2011.
- [19] C. J. Burroughs, S. Benz, and P. D. Dresselhaus, "AC Josephson voltage standard error measurements and analysis," *IEEE Trans. Instrum. Meas.*, vol. 52, no. 2, pp. 542–544, Apr. 2003.
- [20] P. Filipowski, J. Kinard, T. Lipe, and S. Benz, "Correction of systematic errors due to the voltage leads in an ac Josephson voltage standard," *IEEE Trans. Instrum. Meas.*, vol. 58, no. 4, pp. 853–858, Apr. 2009.
- [21] P. S. Filipowski, M. Boecker, S. P. Benz, and C. J. Burroughs, "Experimental determination of the voltage lead error in an ac Josephson voltage standard," *IEEE Trans. Instrum. Meas.*, vol. 60, no. 7, pp. 2387–2392, Jul. 2011.
- [22] H. E. van den Brom and E. Houtzager, "Voltage lead corrections for a pulse-driven ac Josephson voltage standard," *Meas. Sci. Technol.*, vol. 23, Dec. 2012, Art. no. 124007.
- [23] H. E. van den Brom, O. F. O. Kieler, S. Bauer, and E. Houtzager, "AC-DC calibrations with a pulse-driven ac Josephson voltage standard operated in a small cryostat," *IEEE Trans. Instrum. Meas.*, vol. 66, no. 6, pp. 1391–1396, Jun. 2017.
- [24] D. Zhao, H. E. van den Brom, and E. Houtzager, "Mitigating voltage lead errors of an ac Josephson voltage standard by impedance matching," *Meas. Sci. Technol.*, vol. 28, Sep. 2017, Art. no. 095004.
- [25] J. M. Underwood, "Uncertainty analysis for ac-dc difference measurements with the ac Josephson voltage standard," *Metrologia*, vol. 56, Feb. 2019, Art. no. 015012.
- [26] A. E. Fox, P. D. Dresselhaus, A. Rufenacht, A. Sanders, and S. P. Benz, "Junction yield analysis for 10 V programmable Josephson voltage standard devices," *IEEE Trans. Appl. Supercond.*, vol. 25, no. 3, Jun. 2015, Art. no. 1101505.
- [27] J. A. Brevik, N. E. Flowers-Jacobs, A. E. Fox, E. B. Golden, P. D. Dresselhaus, and S. P. Benz, "Josephson arbitrary waveform synthesis with multilevel pulse biasing," *IEEE Trans. Appl. Supercond.*, vol. 27, no. 3, Apr. 2017, Art. no. 1301707.
- [28] WRSPICE Circuit Simulation Software. Whiteley Research Inc., Sunnyvale, CA, USA, Mar. 16, 2019. [Online]: Available: www.wrcad.com